Chinese Chemical Letters 32 (2021) 2274–2278

Contents lists available at ScienceDirect

Chinese Chemical Letters

journal homepage: www.elsevier.com/locate/cclet

Communication

Fluorination strategy enables greatly improved performance for organic solar cells based on polythiophene derivatives

Chenyi Yang[a,b], Shaoqing Zhang[a,b,*], Junzhen Ren[b], Pengqing Bi[b], Xiaotao Yuan[a,*], Jianhui Hou[a,b]

[a] School of Chemistry and Biology Engineering, University of Science and Technology Beijing, Beijing 100083, China
[b] State Key Laboratory of Polymer Physics and Chemistry, Beijing National Laboratory for Molecular Sciences, Institute of Chemistry, Chinese Academy of Sciences, Beijing 100190, China

ARTICLE INFO

Article history:
Received 10 February 2021
Received in revised form 1 March 2021
Accepted 2 March 2021
Available online 4 March 2021

Keywords:
Organic solar cells
Polythiophene derivatives
Fluorination
Aggregation effect
Miscibility

ABSTRACT

The power conversion efficiencies (PCEs) of organic solar cells (OSCs) have reached 18% recently, which have already met the demand of practical application. However, these outstanding results were generally achieved with donor-acceptor (D-A) type copolymer donors, which can hardly fulfill the low-cost large-scale production due to their complicated synthesis processes. Therefore, developing polymer donors with simple chemical structures is urgent for realizing low-cost OSCs. Polythiophene (PT) derivatives are currently regarded as promising candidates for such kind of donor materials, which has been illustrated in many works. In this work, two new alkylthio substituted PT derivatives, P301 and P302, were synthesized and tested as donors in the OSCs using Y5 as the acceptor. In comparison, the introduction of fluorine atoms on the backbone of P302 can not only downshift the energy levels, but also greatly improve the phase separation morphologies of the active layers, which is ascribed to the enhanced aggregation effect and the reduced miscibility with the non-fullerene acceptor. As a result, the P302:Y5-based OSC exhibits a significantly improved PCE of 9.65% than that of P301:Y5-based one, indicating the important role of fluorination in the construction of efficient PT derivative donors.

Organic solar cells (OSCs) have drawn broad attention due to their advantages of light weight, flexibility and suitability for industrial fabrication *via* solution processable methods [1–4]. Different from inorganic solar cells, the light absorption and energy levels of the photovoltaic materials in OSCs can be easily tuned by rational molecular design and modification [5–9]. Therefore, along with the rapid development of the D-A type copolymer donors and A-D-A type non-fullerene acceptors (NFAs), the power conversion efficiencies (PCEs) of single-junction OSCs increased dramatically to 17%–18% recently [10–14]. Although the PCEs have met the demand of practical application of OSCs, the efficient D-A copolymers can hardly fulfill the low-cost large-scale production due to their complicated synthesis and severe purification processes, which seriously hinder the industrialization of OSCs. Therefore, developing photovoltaic materials with simple chemical structures is urgent in the field of OSCs.

Poly(3-hexylthiophene) (P3HT) is well known as a competitive polymer donor for OSCs because it is readily accessible in large quantities with low cost [15,16]. However, P3HT possesses some intrinsic defects such as high-lying highest occupied molecular orbital (HOMO) energy level (−5.0 eV) and narrow light absorption range (< 650 nm), furthermore, its high miscibility with NFAs that impedes the charge transport often leads to the poor photovoltaic performance for P3HT:NFA-based OSCs [17]. Although some studies demonstrated that high open-circuit voltage (V_{OC}) can be achieved in P3HT:NFA-based OSCs by upshifting the energy level of NFAs [18–20], these devices still suffered from relatively low short-circuit current (J_{SC}) and fill factor (FF), which may be ascribed to the limited optical absorption and unfavorable phase separation morphologies of the P3HT:NFAs blends. Keep investigating well-matched P3HT:NFAs is one of the solutions to realize low-cost OSCs with high performance, meanwhile, developing polythiophene (PT) derivatives should be another feasible plan to solve the cost issue [21–24].

* Corresponding authors at: School of Chemistry and Biology Engineering, University of Science and Technology Beijing, Beijing 100083, China.
E-mail addresses: shaoqingz@iccas.ac.cn (S. Zhang), yuanxt@ustb.edu.cn (X. Yuan).

https://doi.org/10.1016/j.cclet.2021.03.006
1001-8417/

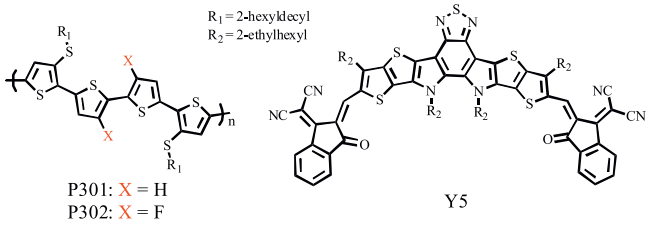

Fig. 1. Chemical structures of donors P301, P302 and acceptor Y5.

In 2016, our group reported an alkoxycarbonyl-functionalized PT derivative named PDCBT, whose energy level is lower than that of P3HT. As a result, a PCE of 10.16% was achieved for PDCBT:ITIC-based device [22]. Then, some encouraging results with PCE over 11% were successively achieved from the OSCs involving PDCBT derivatives [23,24]. For example, Geng *et al.* synthesized PDCBT-Cl by incorporating the Cl atoms to the backbone of PDCBT and achieved a PCE of 12.38% when using ITIC-Th1 as the acceptor [24]. From the results above, the subtle modification on these PT materials can greatly improve the device performance without increasing too much material preparation cost, indicating that PT derivatives are promising donor materials for the future application of OSCs.

The inferior phase separation morphology, mainly caused by the excessive miscibility between donor and acceptor molecules, is responsible for the current disappointing photovoltaic performance of P3HT:NFA-based OSCs, which has been systematically discussed in our previous works [25,26]. Therefore, apart from tuning opto-electronic properties, reducing the miscibility with NFAs should also be considered when design PT derivatives. Herein, we designed and synthesized two new PT derivatives, alkylthio substituted polythiophene (P301) and its difluorinated derivative (P302) (Fig. 1). Compared with P301, P302 has lower HOMO level due to the strong electron-withdrawing effect of fluorine, which is beneficial for higher V_{OC}. More importantly, the introduction of fluorine atoms on thiophene backbones can, on the one hand, form noncovalent interaction between F–S atoms which can effectively enhance the molecular planarity and aggregation behavior of P302; on the other hand, reduce the miscibility between P302 and the NFA, Y5, in blend film to form more favorable phase separation morphology with better interpenetrating charge transport pathways. As a result, the P302:Y5-based device performed more efficient charge generation and transport properties as well as much better photovoltaic performance than the P301-contained counterpart. This work not only reported two new PT derivatives, but also revealed the important role of fluorination in the construction of industrial-oriented simple polymer donors.

Introducing electron donating groups, especially alkoxy and alkylthio substituents, into the β-position of thiophene unit is a commonly-used method to modulate the band gap of the PT-polymers in the early research stage of OSCs [27–29]. Compared to P3HT, Poly[3-alkoxythiophenes] often possess significantly red-shifted absorptions and low oxidation potentials, resulting in higher HOMO levels and thus poor V_{OC} in the OSC. However, for poly[3-(alkylthio)thiophenes], they usually show slightly red-shifted absorption onsets but low-lying HOMO levels in comparison with P3HT, which is desirable for application as donor materials in OSCs. Furthermore, the pre-aggregation effect in solution state for a certain polymer donor is of great importance for achieving favorable phase separation morphology in NFA-based OSCs [30–32]. For PT-polymers which are constructed by rotatable polythiophene as the backbones, stabilizing the conformation by introducing fluorine atom into the β-position of thiophene unit so as to realize strong inter-chain interaction should be a feasible way to form pre-aggregation effect in solution [33–35]. Therefore, we designed the two PT-polymers, P301 and P302, by copolymerizing alkylthio-substituted bithiophene (Ts-Ts) with bithiophene (T-T)/fluoro-substituted bithiophene (Tf-Tf), respectively, and further utilized 2-hexyl-decyl to provide desirable solubility for the two polymers (Scheme S1 in Supporting information). The number-average molecular weight (M_n) of P301 and P302 are 1.52 K and 1.77 K, with polydispersity index (PDI) of 2.15 and 1.81, respectively. The two polymers show good solubility in the commonly-used solvents for OSCs including chlorobenzene, 1,2-dichlorobenzene and chloroform.

To illustrate the effect of F–S interaction on the backbone conformation, the density functional theory (DFT) calculations at the B3LYP/6-31 G (d, p) level were carried out to investigate the optimal geometries of the repeat unit of P301 and P302. As shown in Fig. 2a, both units include two alkylthio-thiophene units and two thiophene (fluorothiophene for P302) units, and present similar optimal geometries. Here we simplified the alkyls to methyl to reduce the cost of calculation. We then calculated the torsional energy between the adjacent conjugated units to study the thermodynamic stability of the backbone conformation of these two polymers. Fig. 2b depicts the torsional energy between the two thiophenes (T-T) in P301 and two fluorothiophenes (Tf-Tf) in P302, respectively. As for stable state, the optimal twist angle is 0° for Tf-Tf segment and 10° for T-T segment. When the twist angle changes from 0° to 180°, Tf-Tf and T-T exhibit metastable states at 140° and 145°, respectively. These two segments also have different torsional energy barriers. The barrier from the stable state to the metastable state is 16.86 kJ/mol for T-T and 21.53 kJ/mol for Tf-Tf. While from the metastable state to the stable state, the barriers are 12.77 kJ/mol and 10.54 kJ/mol for T-T and Tf-Tf, respectively. Additionally, the torsional energy barriers for the other two adjacent rotatable segments in P301 and P302, *i.e.*, two alkylthio thiophenes (Ts-Ts) in both, thiophene-alkylthio thiophene (T-Ts) in P301 *versus* fluorothiophene-alkylthio thiophene (Tf-Ts) in P302, were also estimated. As shown in Fig. S1 (Supporting information), the torsional energy profiles of the other two segments in P302 are almost overlapped with the corresponding ones in P301. The results suggest that F-S interaction enables P302 to form more planar and more stable conformation than P301 even though they

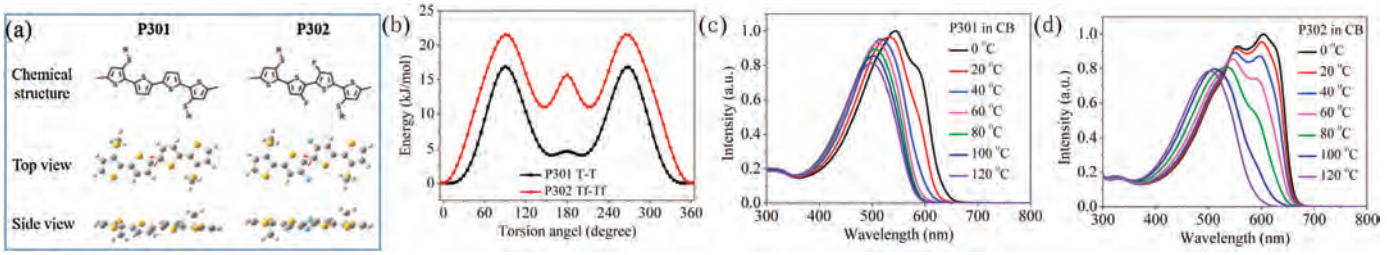

Fig. 2. (a) The optimal geometries of P301 and P302. (b) Torsional energy profiles for T-T and Tf-Tf segments in P301 and P302, respectively. Temperature-dependent UV–vis spectra of (c) P301 and (d) P302 in chlorobenzene solution.

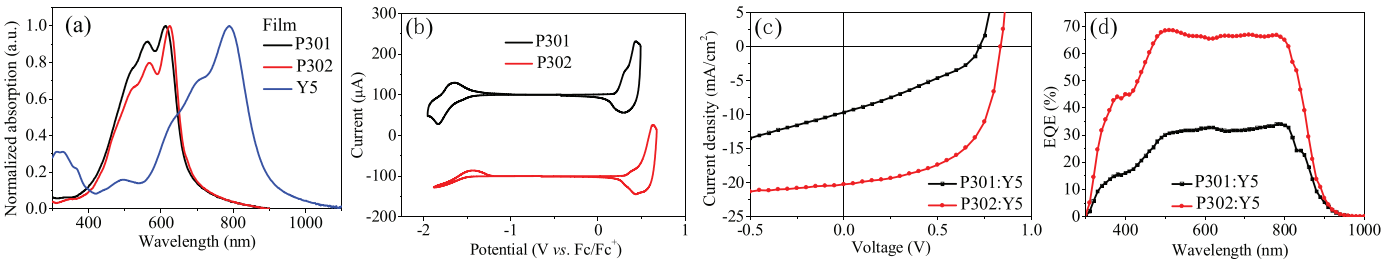

Fig. 3. (a) UV–vis absorption spectra of donors and acceptor in thin film state. (b) CV curves of P301 and P302. (c) *J-V* and (d) EQE curves of devices based on P301 and P302.

have similar optimal geometries, which may contribute to the stronger intermolecular interaction and thus stronger aggregation effect for P302.

Temperature-dependent UV–vis absorption spectroscopy (TD-Abs) was applied to investigate the aggregation effects of the two polymers in solution. As displayed in Figs. 2c and d, these two polymers exhibit similar absorption spectra with onsets at *ca.* 580 nm at the high temperature. When the temperature decreases from 120 °C to 0 °C, the main absorption peaks of both polymer solutions have obvious red-shifted: from 500 nm to 545 nm for P301 and from 503 nm to 603 nm for P302. For P301 solution, an absorption hump caused by intermolecular π-π^* transition appears at *ca.* 600 nm under 20 °C. While for P302 solution, the hump can be initially observed at 100 °C and increases gradually to a shoulder peak as the temperature reduces. The TD-Abs results demonstrate that P302 has stronger aggregation effect in solution state than P301, which may be caused by the more planar backbone conformation of P302. We can then reasonably infer that the strong interchain interaction for P302 solution is conducive to achieve more desirable nanoscale phase separation during spin-coating process, thus result in better photo-induced charge generation and transport properties for corresponding NFA-based devices.

The molecular packing characteristics of these two polymers in solid state were also studied by grazing incident wide-angle X-ray scattering (GIWAXS) measurements. As shown in Fig. S2, P301 film has weak (010) π-π stacking diffraction signals in both in-plane (IP) and out-of-plane (OOP) directions, whereas P302 film prefers face-on orientation with pronounced (010) diffraction peak in OOP direction. The more ordered molecular packing of P302 should be ascribed to its stronger planarity.

The UV–vis absorption spectra of these two polymers in film state are displayed in Fig. 3a. In comparison with P301, P302 possesses a stronger and 10 nm redshifted absorption shoulder at long wavelength direction attributed to interchain π-π^* transition, indicating the stronger intermolecular interaction of P302. The two polymers have almost the same absorption onset at *ca.* 680 nm, corresponding to an optical bandgap of 1.82 eV. The HOMO and the lowest unoccupied molecular orbital (LUMO) energy levels of these two polymers were calculated from the onset of oxidation and reduction potentials measured by electrochemical cyclic voltammetry (CV, Fig. 3b), respectively. As a result, the calculated E_{HOMO} and E_{LUMO} are −5.02 eV and −3.18 eV for P301, −5.12 eV and −3.29 eV for P302, respectively. The strong electron-withdrawing effect of fluorine atoms can lower the energy levels of P302, which is commonly observed in many NFA design cases as well [36,37].

The photovoltaic properties of these two polymers were tested in conventional OSC devices with structure of ITO/PEDOT:PSS/active layer/PFN-Br/Al, where Y5 was selected as the acceptor in consideration of the complementary absorption and matched energy levels with donors [38]. Fig. 3c depicts the current density-voltage (*J*–*V*) curves of the optimized devices under the illumination of AM 1.5 G 100 mW/cm^2, and the corresponding photovoltaic parameters are listed in Table 1. The P301-based device exhibits a

Table 1
Photovoltaic parameters of the P301:Y5- and P302:Y5-based OSCs.

Active layer	V_{OC} (V)	J_{SC} (mA/cm^2)	FF	PCE (%)
P301:Y5	0.72	9.67 (9.45)[a]	0.33	2.33 (2.25 ± 0.07) [b]
P302:Y5	0.84	20.24 (19.80)[a]	0.57	9.65 (9.46 ± 0.11) [b]

[a] Calculated J_{SC} from the EQE spectra shown in Fig. 3d.
[b] All average values with standard deviations were calculated from more than ten devices.

modest PCE of 2.33% with a V_{OC} of 0.72 V, a J_{SC} of 9.67 mA/cm^2 and a FF of 0.33, while all of the three parameters are greatly improved in P302-based counterpart with a V_{OC} of 0.84 V, a J_{SC} of 20.24 mA/cm^2 and a FF of 0.57, affording a much higher PCE of 9.65%. The enhanced V_{OC} is mainly ascribed to the low-lying HOMO energy level of P302, and the higher J_{SC} and FF may be attributed to the superior phase separation morphology of P302:Y5 blend, which will be discussed later. The external quantum efficiency (EQE) curves of these two devices are displayed in Fig. 3d. When compared with P301-based device, the P302-based one exhibits much higher EQE in the whole photo response range with a very flat EQE band over 65% from 480 nm to 800 nm due to the perfect complementary absorption with Y5 (Fig. 3a), indicating the efficient photoelectron conversion in P302-based-device. In addition, the J_{SC} values calculated from the integration of the EQE curves are 9.45 and 19.80 mA/cm^2 for P301- and P302-based devices, respectively, which agree well with the J_{SC} values obtained from the *J-V* measurements within 3% mismatch.

From the *J-V* results, we can clearly observe that the photocurrent (J_{ph}) of P301:Y5-based device increases with the increase of reverse bias, suggesting the impeded charge separation or transport processes in this device, which can be intuitively investigated by measuring the dependence of the photocurrent on the effective voltage (V_{eff}). J_{ph} equals J_L-J_D, where J_L and J_D are the current densities under illumination and in the dark, respectively. V_{eff} is defined as V_0-V, where V_0 is the voltage when J_{ph} is zero and V is the applied voltage. For OSCs, J_{ph} will reach saturation (J_{sat}) if V_{eff} is high enough, and the exciton dissociation probability (P_{diss}) can be defined as J_{ph}/J_{sat} [39]. As plotted in Fig. 4a, the P_{diss} values are 53% and 84% for P301- and P302-based devices, respectively, indicating the more efficient charge separation and collection in P302-based device, which accounts for the improved PCE.

The J_{SC} of each optimized OSCs under different illumination intensities (P_{light}) was measured to study the charge recombination behavior. Generally, the relationship between J_{SC} and P_{light} can be expressed as a power-law dependence of $J_{SC} \propto P_{light}^{S}$, where S should be equal to 1 if all free carriers are swept out and collected at the electrodes without recombination [40]. As depicted in Fig. 4b, the S value of P301-based device is 0.79 while the P302-based one exhibits a higher value of 0.90, implying that the bimolecular recombination is more suppressed in P302-based device. The carrier mobilities were also evaluated by the space charge limited current (SCLC) method with the device structure of

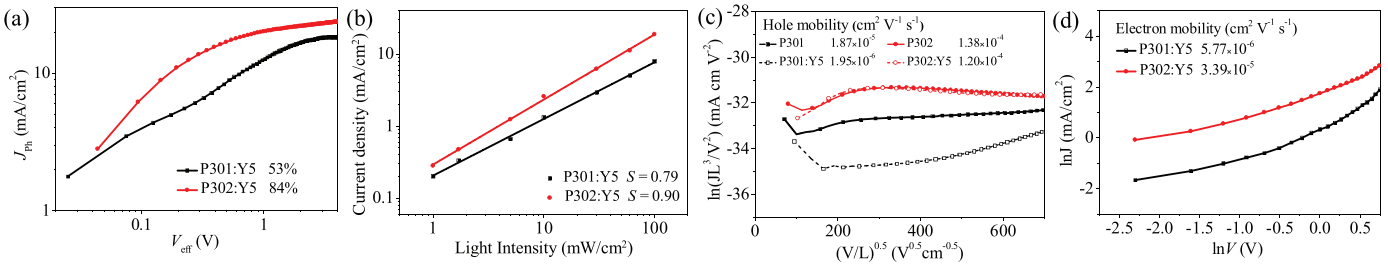

Fig. 4. (a) J_{ph} *versus* V_{eff} characteristics and (b) dependence of J_{SC} on light intensity for P301- and P302-based devices. (c) The hole and (d) electron mobilities measured by the SCLC method.

ITO/PEDOT:PSS/active layer/Au for hole mobility (μ_h) and ITO/ZnO/active layer/Al for electron mobility (μ_e), respectively. As shown in Figs. 4c and d, the P302 neat film presents one order of magnitude higher μ_h (1.38×10^{-4} cm^2 V^{-1} s^{-1}) than P301 (1.87×10^{-5} cm^2 V^{-1} s^{-1}), which should be ascribed to the more ordered molecular packing of P302 polymers stemming from the enhanced intermolecular π-π interaction. As for blend films, both μ_h and μ_e of the P302-based film (9.75×10^{-5} and 3.39×10^{-5} cm^2 V^{-1} s^{-1}) are much higher than those of the P301-based one (1.95×10^{-6} and 5.77×10^{-6} cm^2 V^{-1} s^{-1}), indicating that the charge transport process in P302-based film is more efficient. The less carrier recombination and higher charge mobilities can well explain the higher J_{SC} and FF of P302-based device.

To gain more insight into the reasons for why these two polymers exhibit such different photovoltaic properties in OSC devices, the differential scanning calorimetry (DSC) measurements were carried out to investigate the miscibility between donors and acceptor. However, as shown in Fig. S3 (Supporting information), P301, P302 and Y5 all exhibit amorphous state since neither endothermic nor exothermic peaks can be observed on their DSC curves, making it impossible to judge the miscibility of their blends through DSC method. As the donor polymer mainly interact with the end groups of a small molecular acceptor, a crystalline molecule TT-IC imitating the end group of Y5 was employed to blend with P301 and P302 in DSC measurements, respectively. TT-IC was synthesized according to our previous study [26]. As displayed in Fig. 5a, TT-IC exhibits strong crystallinity with melting and crystallizing temperatures (T_m and T_c) about 209 °C and 119 °C, respectively. As for blends with weight ratio of 1:0.6 (this ratio is derived from 1:1 used in the corresponding Y5-based OSC devices), no phase transition signals can be observed for P301:TT-IC blend; whereas P302:TT-IC blend shows distinct endothermic and exothermic peaks near the T_m and T_c of TT-IC, respectively, which should belong to the separated TT-IC phase in blend. When the weight ratio changes to 1:1, the endothermic and exothermic peaks of P301:TT-IC blend appear as well, indicating that TT-IC begins to form an individual phase for its content in P301 phase has reached saturation. The DSC results suggest that TT-IC prefers to form individual phase when blended with P302, indicating the less miscibility of the P302:TT-IC blend when compared with the P301:TT-IC-based one.

The miscibility between TT-IC and these two polymers can also be intuitively observed by probing the surface morphologies of their blend films through atomic force microscopy (AFM). As displayed in Fig. S4 (Supporting information), P301 and P302 neat films possess relatively smooth surface while TT-IC presents oversize aggregation in the film state. The AFM images of blend films are depicted in Fig. 5b. Under the weight ratio of 1:0.6, little TT-IC crystal is precipitated on the surface of the P301:TT-IC film while a large amount of flaky crystal can be observed on the P302:TT-IC-based one. As the composition of TT-IC increases, both films are almost covered with TT-IC crystal. The observations from AFM are highly consistent with the conclusion drawn from the DSC tests, that is, in comparison with P301, P302 exhibits lower miscibility with TT-IC. The same is true when replacing TT-IC with Y5, which can be verified by AFM as well. As shown in Fig. 5c, nanoscale aggregation can be distinguished on the surface of P302:Y5-based blend film with root-mean-square surface roughness (R_q)

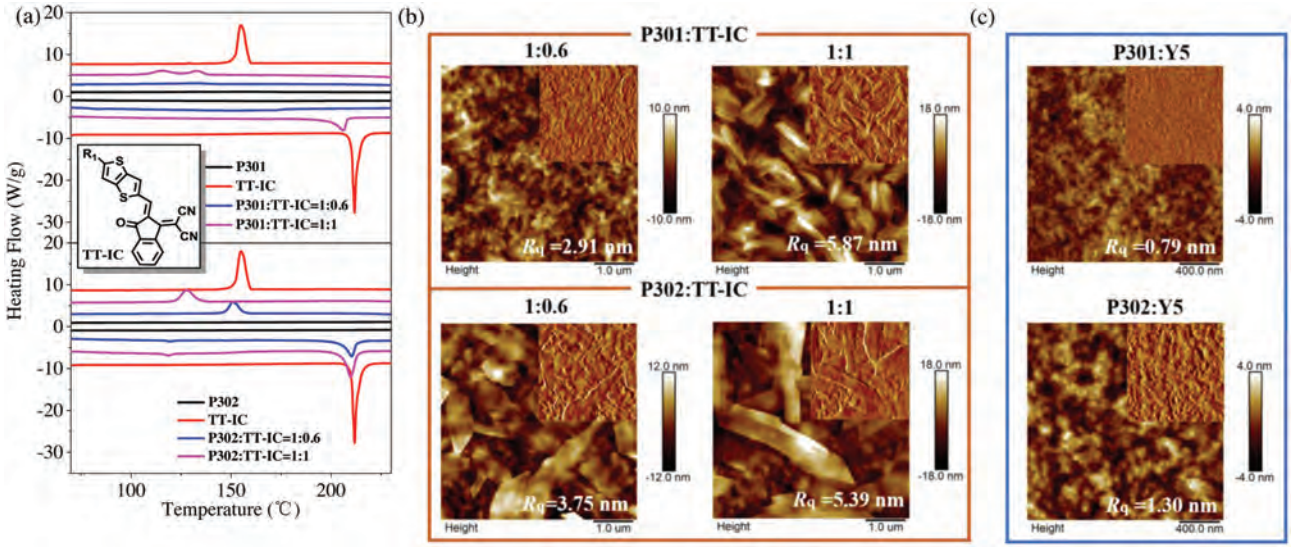

Fig. 5. (a) DSC curves of P301, P302 and TT-IC neat materials, P301:Y5 and P302:Y5 blends at weight ratios of 1:0.6 and 1:1 (Exo up). Inset: the chemical structure of TT-IC. (b) AFM images of P301:TT-IC and P302:TT-IC blend films at weight ratios of 1:0.6 and 1:1 (5×5 μm^2). (c) AFM images of P301:Y5 and P302:Y5 blend films (2×2 μm^2).

of 1.30 nm, while P301:Y5-based one has a homogeneous surface with R_q of 0.79 nm. Fig. S5 (Supporting information) displays the transmission electron microscopy (TEM) results of these two blend films. In comparison with P301:Y5-based film, P302:Y5-based one exhibits distinct phase separation morphology, which agrees well with the results observed from AFM. Under the synergistic effect of enhanced aggregation effect and weakened miscibility with Y5, blend films based on P302 possesses superior phase separation morphologies, which accounts for the significantly improved J_{SC} and FF for the corresponding devices.

In conclusion, we synthesized two PT derivatives P301 and its fluorinated derivative P302 as donors for OSCs. Introducing fluorine onto the thiophene conjugated backbone of P302 can not only downshift the energy levels thus output higher V_{OC}, but also, more importantly, greatly improve the phase separation morphologies of active layers, which is a result of the synergistic effect of two factors: first, the F-S noncovalent interaction in P302 endows it a more planar conformation thus stronger aggregation effect; second, fluorination can effectively reduce the miscibility between P302 and end groups of acceptors. As a result, when using Y5 as acceptor, all the photovoltaic parameters of device based on P302 are dramatically improved when compared with the P301-based one, leading to a significant increase in PCE from 2.33% to 9.65%. Our results reveal the importance of fluorination strategy in constructing high-performance PT derivative donors for OSCs.

Declaration of competing interest

The authors declare that they have no known competing financial interests or personal relationships that could have appeared to influence the work reported in this paper.

Acknowledgments

The authors would like to acknowledge the financial support from the Basic and Applied Basic Research Major Program of Guangdong Province (No. 2019B030302007), the National Natural Science Foundation of China (Nos. 21835006, 91633301 and 22075017), the Fundamental Research Funds for the Central Universities, China (No. FRF-TP-19-047A2) and Beijing National Laboratory for Molecular Sciences (No. BNLMS-CXXM-201903).

Appendix A. Supplementary data

Supplementary material related to this article can be found, in the online version, at doi:https://doi.org/10.1016/j.cclet.2021.03.006.

References

[1] R. Søndergaard, M. Hösel, D. Angmo, T.T. Larsen-Olsen, F.C. Krebs, Mater. Today 15 (2012) 36–49.
[2] O. Inganas, Adv. Mater. 30 (2018) e1800388.
[3] H. Kang, G. Kim, J. Kim, et al., Adv. Mater. 28 (2016) 7821–7861.
[4] G. Li, R. Zhu, Y. Yang, Nat. Photonics 6 (2012) 153–161.
[5] Y. Li, Acc. Chem. Res. 45 (2012) 723–733.
[6] H. Yao, L. Ye, H. Zhang, et al., Chem. Rev. 116 (2016) 7397–7457.
[7] J. Hou, O. Inganas, R.H. Friend, F. Gao, Nat. Mater. 17 (2018) 119–128.
[8] A. Wadsworth, M. Moser, A. Marks, et al., Chem. Soc. Rev. 48 (2018) 1596–1625.
[9] X. Xu, G. Zhang, Y. Li, Q. Peng, Chin. Chem. Lett. 30 (2019) 809–825.
[10] W. Zhao, D. Qian, S. Zhang, et al., Adv. Mater. 28 (2016) 4734–4739.
[11] S. Zhang, Y. Qin, J. Zhu, J. Hou, Adv. Mater. 30 (2018) e1800868.
[12] J. Yuan, Y. Zhang, L. Zhou, et al., Joule 3 (2019) 1140–1151.
[13] Y. Cui, H. Yao, J. Zhang, et al., Adv. Mater. (2020) e1908205.
[14] Q. Liu, Y. Jiang, K. Jin, et al., Sci. Bull. 65 (2020) 272–275.
[15] R. Po, A. Bernardi, A. Calabrese, et al., Energy Environ. Sci. 7 (2014) 925–943.
[16] S. Holliday, R.S. Ashraf, A. Wadsworth, et al., Nat. Commun. 7 (2016) 11585.
[17] A. Marrocchi, D. Lanari, A. Facchetti, L. Vaccaro, Energy Environ. Sci. 5 (2012) 8457–8474.
[18] P. Ye, Y. Chen, J. Wu, et al., Mater. Chem. Front. 3 (2019) 64–69.
[19] B. Xiao, A. Tang, L. Cheng, et al., Sol. RRL 1 (2017) 1700166.
[20] F. Liu, J. Zhang, Z. Zhou, et al., J. Mater. Chem. A 5 (2017) 16573–16579.
[21] Q. Xu, C. Chang, W. Li, et al., Acta Phys. Chim. Sin. 35 (2019) 268–274.
[22] Y. Qin, M.A. Uddin, Y. Chen, et al., Adv. Mater. 28 (2016) 9416–9422.
[23] H. Yao, D. Qian, H. Zhang, et al., Chin. J. Chem. 36 (2018) 491–494.
[24] Q. Wang, M. Li, X. Zhang, et al., Macromolecules 52 (2019) 4464–4474.
[25] C. Yang, N. Liang, L. Ye, et al., Org. Electron. 68 (2019) 15–21.
[26] C. Yang, S. Zhang, J. Ren, et al., Energy Environ. Sci. 13 (2020) 2864–2869.
[27] X. Wu, T. Chen, R.D. Rieke, Macromolecules 29 (1996) 7671–7677.
[28] C.A. Cutler, A.K. Burrell, D.L. Officer, C.O. Too, G.G. Wallace, Synth. Met. 128 (2002) 35–42.
[29] L. Huo, Y. Zhou, Y. Li, Macromol. Rapid Commun. 30 (2009) 925–931.
[30] Y. Liu, J. Zhao, Z. Li, et al., Nat. Commun. 5 (2014) 5293.
[31] D. Qian, L. Ye, M. Zhang, et al., Macromolecules 45 (2012) 9611–9617.
[32] Z. Zheng, H. Yao, L. Ye, et al., Mater. Today 35 (2020) 115–130.
[33] S. Zhang, Y. Qin, M.A. Uddin, et al., Macromolecules 49 (2016) 2993–3000.
[34] G. Yang, Z. Li, K. Jiang, et al., Sci. China Chem. 60 (2017) 545–551.
[35] J.T. Blaskovits, T. Bura, S. Beaupre', et al., Macromolecules 50 (2017) 162–174.
[36] A. He, Y. Qin, W. Dai, D. Zhou, J. Zou, Chin. Chem. Lett. 30 (2019) 2263–2265.
[37] W. Zhao, S. Li, H. Yao, et al., J. Am. Chem. Soc. 139 (2017) 7148–7151.
[38] J. Yuan, Y. Zhang, L. Zhou, et al., Adv. Mater. 31 (2019) 1807577.
[39] J.L. Wu, F.C. Chen, Y.S. Hsiao, et al., ACS Nano 5 (2011) 959–967.
[40] M. Lenes, M. Morana, C.J. Brabec, P.W.M. Blom, Adv. Funct. Mater. 19 (2009) 1106–1111.